

# BAYESIAN JOINT MODELING OF CHEMICAL STRUCTURE AND DOSE RESPONSE CURVES

BY KELLY R. MORAN\*, DAVID DUNSON\* AND AMY H. HERRING\*

*Duke University\**

Today there are approximately 85,000 chemicals regulated under the Toxic Substances Control Act, with around 2,000 new chemicals introduced each year. It is impossible to screen all of these chemicals for potential toxic effects either via full organism *in vivo* studies or *in vitro* high-throughput screening (HTS) programs. Toxicologists face the challenge of choosing which chemicals to screen, and predicting the toxicity of as-yet-unscreened chemicals. Our goal is to describe how variation in chemical structure relates to variation in toxicological response to enable *in silico* toxicity characterization designed to meet both of these challenges. With our Bayesian partially Supervised Sparse and Smooth Factor Analysis (BS<sup>3</sup>FA) model, we learn a distance between chemicals targeted to toxicity, rather than one based on molecular structure alone. Our model also enables the prediction of chemical dose-response profiles based on chemical structure (that is, without *in vivo* or *in vitro* testing) by taking advantage of a large database of chemicals that have already been tested for toxicity in HTS programs. We show superior simulation performance in distance learning and modest to large gains in predictive ability compared to existing methods. Results from the high-throughput screening data application elucidate the relationship between chemical structure and a toxicity-relevant high-throughput assay. An **R** package for BS<sup>3</sup>FA is available online at <https://github.com/kelrenmor/bs3fa>.

**1. Introduction.** Daily life involves being exposed to a variety of chemical substances from diverse sources and at varying concentrations. A myriad of legislation and regulatory bodies work to assess consumer and industrial products for toxicity and reduce exposure risk. The Toxic Substances Control Act (TSCA), passed by Congress in 1976 and administered by the US Environmental Protection Agency (EPA), regulates the bulk of<sup>1</sup> new and existing chemicals in the United States (US). When the TSCA was enacted, around 60,000 chemicals were grandfathered into the program and effectively considered safe for use. The EPA has struggled to catch up on this backlog while also keeping up with the rate of new introductions (roughly 2,000 chemicals per year) as they assess chemicals for potential toxicity. High-throughput screening methods have proved vital to this effort as they allow researchers to quickly conduct millions of tests.

The EPA’s Toxicity Forecaster (ToxCast) research program, in which thousands of chemicals are tested in more than 700 high-throughput assay endpoints, is used to prioritize, screen and evaluate chemicals for potential toxic effects (Dix et al., 2006; Judson et al., 2009; Kavlock et al., 2012). However, even high-throughput toxicity screening (HTS) programs, which allow for the relatively cheap and fast collection of dose-response information via *in vitro* studies rather than full organism

---

*Keywords and phrases:* Dimension reduction, Distance learning, Functional prediction, High-throughput screening, Toxicity, ToxCast, QSAR

<sup>1</sup>Exceptions regulated under different legislation include foods and food additives, drugs, cosmetics, pesticides, tobacco products, research substances used in small quantities, and radioactive materials and waste.

*in vivo* studies, are still too slow and expensive to be able to study all chemicals. *In silico* studies, i.e. those performed via computer modeling rather than in the lab, can be used to guide the design of and supplement the results from lab-based studies. Specifically, the characterization of an activity relevant chemical distance *in silico* enables more targeted design of further *in vitro* studies, increasing the efficiency of resource allocation. In addition, predicting toxicity via such studies helps bridge the gap between the number of chemicals of interest and the number with known toxicological profiles.

The goal of this work is to make inferences about how variation in chemical structure relates to variation in toxicological response. Sparse function-on-scalars regression models (Chen, Goldsmith and Ogden, 2016; Barber et al., 2017; Fan and Reimherr, 2017; Kowal and Bourgeois, 2018) do this in a limited way by selecting the important chemical structure features and giving them appropriate coefficients or weights. Because there are many redundant and highly correlated structure features (see Figure 1), a PCA-esque approach that introduces latent factors related to the major directions of variation in the molecular structure is more informative than such penalized regression approaches. However, simply performing PCA or other unsupervised dimension reduction approaches on the chemical structure ignores the distinction between *overall* variation and *toxicity-relevant* variation in the molecular structure. A supervised dimension reduction approach, on the other hand, provides a coherent and flexible framework within which to describe the relationship between molecular variation and activity variation via a shared latent subspace.

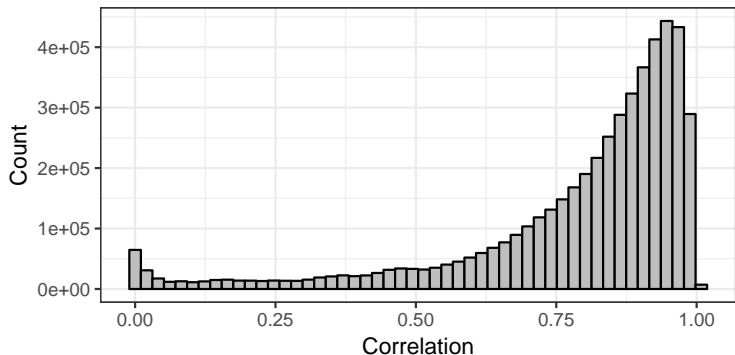


Fig 1: Pairwise correlation between each of the 777 molecular descriptors in ToxCast for the chemicals profiled.

Dose response data and molecular structure are the two sources of information in ToxCast relevant to addressing our goal. Explicitly, chemical  $i$  in ToxCast has two relevant pieces of information: the vector of response observations at  $D$  doses  $\mathbf{y}_i = [y_i(d_1), \dots, y_i(d_D)]'$ , and the vector of  $S$  molecular features  $\mathbf{x}_i = [x_{i1}, \dots, x_{iS}]'$ . Observations  $\mathbf{y}_i$  are sparse, noisy, and not on a regular grid. For an example see Figure 2; Chlorobenzilate has 54 observations at 11 unique doses, yet 5-Methyl-1H-benzotriazole only has 3 doses with one observation each. Not all aspects of the feature space (i.e. not all entries in  $\mathbf{x}_i$ ) are likely to be relevant to the toxicological response.

The specific high throughput assay analyzed here is the AttaGene pregnane X receptor (PXR) assay. This assay targets the PXR via the xenobiotic pathway and has been shown to be related to the body’s response to toxic substances (Kliwer, Goodwin and Willson, 2002). The tool used to quantitatively summarize a chemical’s molecular structure is Mold2 (Hong et al., 2008), which generates a set of 777 numeric descriptors using the simplified molecular-input line-entry system (SMILES) specification (Weininger, 1988). See Figure 3 for select Mold2 output for an example chemical, and (Hong et al., 2012) for a discussion of the use of Mold2 in Quantitative Structure–Activity

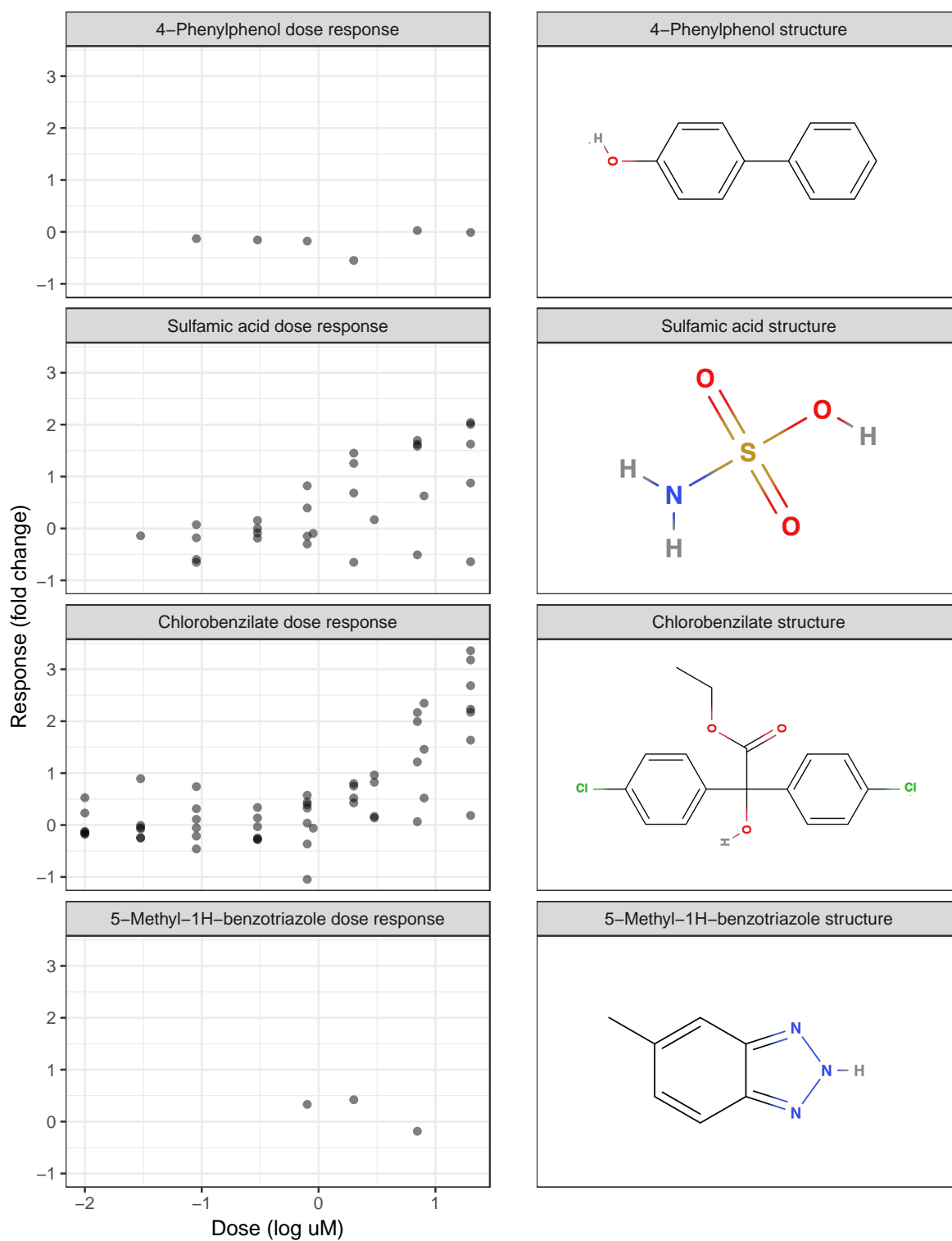


Fig 2: Left: Dose response data for example chemicals from the ToxCast ATG PXR assay (i.e.,  $y_i$ ). Right: 2D chemical structure diagrams for example chemicals (converted from SMILES into  $x_i$  using the Mold2 software).

Relationship (QSAR) models.

In order to coherently model both structural and toxicological response variation, we propose a Bayesian partially Supervised Sparse and Smooth Factor Analysis (BS<sup>3</sup>FA) model. The model assumes structured variation in the molecular features  $\mathbf{x}_i$  is driven by two sets of latent factors: call these  $F_{x\text{-specific}}$  and  $F_{\text{shared}}$ .  $F_{x\text{-specific}}$  is unrelated to the toxicological response and is responsible for structured molecular variability that does not impact toxicity.  $F_{\text{shared}}$  is assumed to drive variation in the toxicological response  $\mathbf{y}_i$ , and thus is responsible for structured molecular variability that *does* impact toxicity. The directions spanned by these two sets of latent factors can be thought of as the “toxicity-irrelevant” and “toxicity-relevant” spaces, respectively.

Chemical similarity can be characterized by proximity in this latent toxicity-relevant space, enabling a measure of distance with uncertainty quantification that is adapted to the particular response space of interest. Such a metric is powerful because (1) it is based on a subspace driving variation in activity, whereas proximity with respect to the full set of molecular descriptors does not necessarily mean proximity with respect to activity (Martin, Kofron and Traphagen, 2002; Nikolova and Jaworska, 2003), and (2) it is purely statistically derived, requiring no knowledge of the fundamental chemical and biological processes responsible for the activity, as such information is not always available. Such an activity-relevant distance metric could be used by toxicologists in the design of diverse chemical libraries or to select new compounds to augment a screening collection such as ToxCast.

As with function-on-scalars regression approaches, the BS<sup>3</sup>FA model allows for the prediction of activity profiles for chemicals that have not yet been screened in ToxCast. It does so by embedding the full set of molecular features for a new chemical into the latent toxicity-relevant feature space  $F_{\text{shared}}$ , and then projecting this embedding out to the activity space. The predicted dose-response profiles can be used to generate point and interval estimates for common univariate toxicological outcomes of interest, such as 50% activity concentration (AC50), maximum activity, or the area under curve (AUC), which can be used in place of the as of yet unobserved *in vitro* results for that chemical.

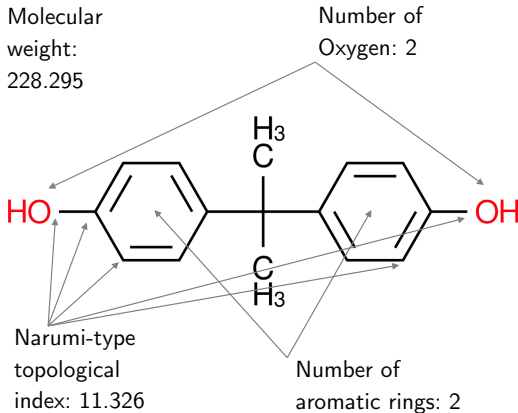


Fig 3: Numeric values for select Mold2 traits of Bisphenol A (BPA). The chemical formula for BPA is  $C_{15}H_{16}O_2$ , and its SMILES descriptor is CC(C)(C1=CC=C(C=C1)O)C2=CC=C(C=C2)O.

The rest of the paper is organized as follows. First, we describe existing and potential approaches to modeling chemical structure and activity. Then, the BS<sup>3</sup>FA model is described and its performance is compared to that of existing algorithms on simulated data sets. Next, a detailed analysis of the

motivating application data set is considered, where the BS<sup>3</sup>FA model is run with Mold2 chemical features and the Attagene PXR assay from the ToxCast data set as input data. Finally, the results are discussed and future areas of research are highlighted.

**2. Background.** QSAR models (see Figure 4) are based on the assumption that chemicals with similar features are likely to have similar effects. The ToxCast data poses two main challenges for QSAR modeling. First, it is often not trivial to characterize similarity in activity-relevant chemical feature space well (Martin, Kofron and Traphagen, 2002; Nikolova and Jaworska, 2003). Second, the majority of QSAR models aim to relate structure to a *summary* of the data across times/doses (e.g., (Liu et al., 2011; Patel et al., 2014)) rather than to the *full* dose response curves.

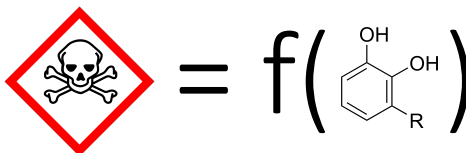


Fig 4: Quantitative Structure-Activity Relationship (QSAR) models predict toxicity as a function of chemical structure.

We discuss these considerations in the context of existing QSAR models and other related approaches not yet applied to QSAR models. To the authors’ knowledge, no existing approaches are able to address the challenge of learning a low-dimensional representation for multivariate feature data  $\mathbf{x}_i$  partially supervised by sparse functional data  $\mathbf{y}_i$ .

**2.1. QSAR approaches for dose response profiles.** Two existing QSAR approaches have attempted to relate molecular descriptors to full dose response curves (Low-Kam et al., 2015; Wheeler, 2019). In (Low-Kam et al., 2015), a Bayesian regression tree is defined over functions where each leaf represents a different dose-response surface. This method was used to learn about the relationship between chemical properties and observed dose-response. However, the model lacks the ability to scale to the numbers of chemicals and molecular descriptors considered here. Furthermore, predictive performance was found to be lacking in leave-one-out analysis. Finally, the code was designed under the assumption that each chemical would be tested at the same doses with the same number of replicates at each dose.

The Bayesian Additive Adaptive Basis Tensor Product (BAABTP) model (Wheeler, 2019) is designed purely for prediction. It learns basis functions via independent Gaussian process (GP) priors over the molecular structure space and the dose space. In the model, step one is to perform PCA on the set of Mold2 chemical descriptors. Step two is to use the principal feature space explaining 95% of the variation in this Mold2 descriptor set as the input to the distance kernel for the molecular structure GPs.

The BAABTP model has two major problems, both stemming from the Gaussian process prior over chemical structure. First, the model becomes computationally intractable when the number of chemicals increases past a few thousand— the number of chemicals tested in the ATG PXR assay has increased from under 1,000 up to nearly 4,000 in the time since the data were analyzed in (Wheeler, 2019), and this number will only continue to grow. Second, the GP priors over chemical structure rely on a concept of molecular distance based on total, rather than toxicity-relevant, variability. Mold2 descriptors are a numeric representation of the 2D structure of a chemical. Thus,

while the leading principal components (PCs) account for the majority of structural variability across chemicals, these leading PCs may not be those most relevant to toxicity. Figure 5 illustrates this phenomenon, showing that chemicals may be close in PCA-based structure space but distant in response space. In other words, similarity in directions of highest structural variability does not necessarily correspond to similarity in directions of highest activity variability.

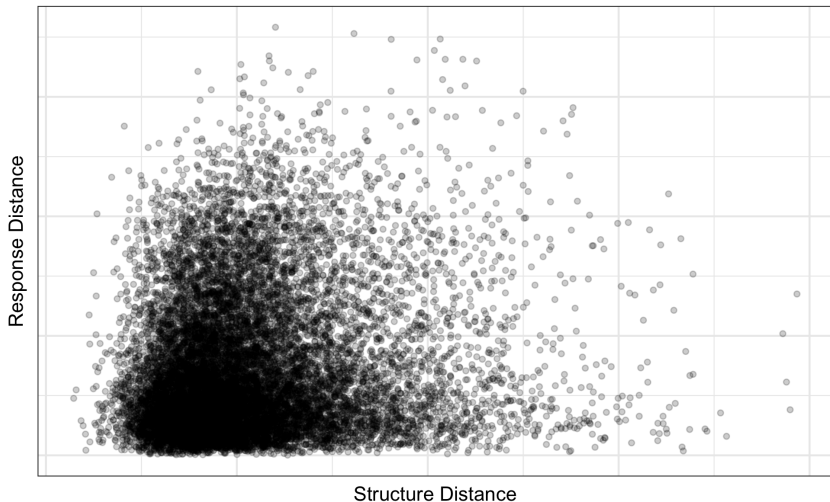


Fig 5: Relationship between chemical “structure distance” and chemical “activity distance” when PCA and functional PCA (FPCA) are performed *independently* on the Mold2 chemical structures and the ToxCast dose response curves. Each point on the graph shows the Euclidean distance between the (functional) principal component scores accounting for 95% of the variability in the data for one pair of chemicals on the ( $y$ -)  $x$ -axis.

**2.2. Towards the proposed approach.** Supervised and sparse functional PCA (supSFPCA) (Li, Shen and Huang, 2016) defines a hierarchical model to provide supervision for dimension reduction of functional data by another multi-output data source. A small modification to the penalty term used in this algorithm would allow for the opposite relation (i.e., to supervise the dimension reduction of the feature data  $\mathbf{x}_i$  by functional dose-response data  $\mathbf{y}_i$ ), but the larger issue is that the supSFPCA algorithm is designed such that the algorithm finds directions that maximize *unexplained* variability in  $\mathbf{x}_i$  (that is, what isn’t accounted for by  $\mathbf{y}_i$ ) rather than finding directions that maximize variability *explained* by  $\mathbf{y}_i$ . As such, this algorithm is of little use for prediction or for learning about directions of variability of most relevance for toxicity.

Our approach was inspired by the conceptual goal of separating variability shared by  $\mathbf{x}_i$  and  $\mathbf{y}_i$  into toxicity-relevant, toxicity-irrelevant, and noise components, similar to the idea behind the Joint and Individual Variation Explained (JIVE) method (Lock et al., 2013). Unlike JIVE, modeling takes place within a Bayesian framework for unified parameter estimation, prediction, and uncertainty quantification about posterior summaries of interest, and model components are identifiable. We utilize similar tools as the function-on-scalars regression of (Kowal and Bourgeois, 2018), implementing sparsity-inducing coefficient-level priors to account for the high-dimensional predictors, learning a flexible basis for the functional response, and imposing ordered sparsity so as to reduce the impact of the choice of latent subspace dimension.

Like many of the approaches described in the previous sections, our model is able to predict the dose-response profiles for new chemicals. Unlike previous models, our model is able to learn a toxicity-relevant subspace underlying variation in both the chemical structure and toxicological

response. This subspace can be used to describe a statistically-driven activity-relevant distance between chemicals. It can also provide insight into how toxicity-relevant variability manifests across both molecular structure and dose-response profiles.

**3. BS<sup>3</sup>FA model.** Figure 6 gives a visual representation of the BS<sup>3</sup>FA model. BS<sup>3</sup>FA is able to: (1) learn a linear low dimensional latent space underlying both molecular structure and activity, (2) develop a distance metric for chemicals relying only on molecular structures relevant to toxicity, (3) handle responses observed at a sparse, irregularly spaced set of doses, and (4) enable activity predictions for chemicals having no observed dose response information.

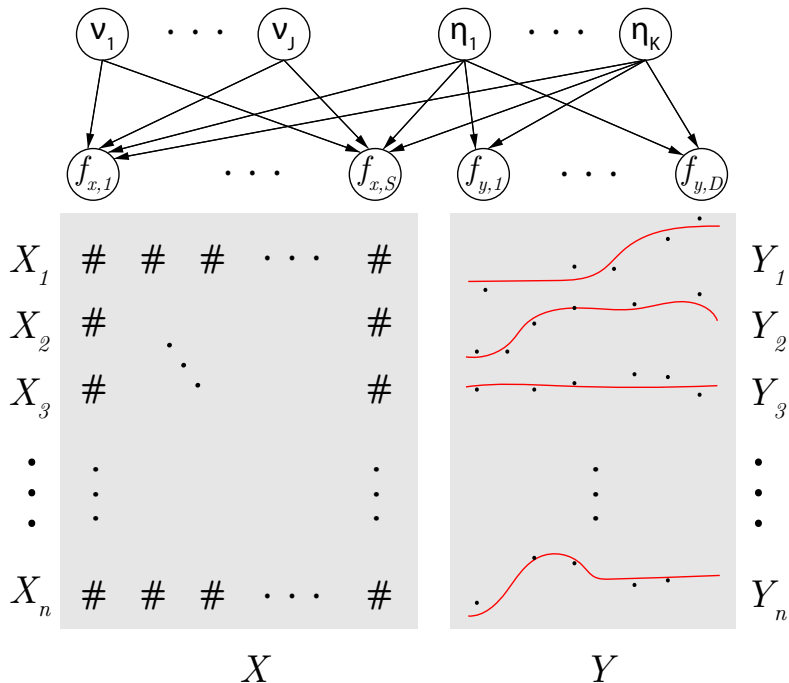


Fig 6: Visual representation of the BS<sup>3</sup>FA model. Entries in  $X$  are the chemical feature descriptors from Mold2, while entries in  $Y$  are noisy realizations of an underlying smooth dose response curve. Observations  $f_{x,1}, \dots, f_{x,S}$  are the true mean of the chemical features and  $f_{y,1}, \dots, f_{y,D}$  are the true mean of the dose response values. Latent variables  $\eta_1, \dots, \eta_K$ , the underlying toxicity-relevant factors, are shared, and  $\nu_1, \dots, \nu_K$ , the underlying toxicity-irrelevant factors, are specific to the chemical features. Arrows denote probabilistic dependency.

**3.1. Model specification.** **The characteristics of chemical structure and toxicological response can likely be summarized using fewer descriptors.** As shown in Figure 1, many molecular descriptors tend to exhibit high correlation. Furthermore, their realized value can often be attributed to some underlying trait of the molecule (e.g., many descriptors are largely driven by molecule size; the descriptors number of carbon, number of oxygen, molecular weight, and number of atoms in the molecule all have pairwise correlation above 0.9). Similarly, dose response profiles exhibit a somewhat limited range of shapes, suggesting possibly a few underlying functional “building blocks” comprising variation in activity.

Factor modeling is a means by which to model variability in high dimensional data via an underlying lower dimensional subspace. For some set of observations  $\{z_i\}_{i=1}^N$ , where  $z_i$  is the  $P$ -dimensional



vector of measurements for observation  $i$ , the traditional (non-joint) factor model is:

$$(1) \quad \begin{aligned} \mathbf{z}_i &= \Lambda \boldsymbol{\eta}_i + \boldsymbol{\epsilon}_i, \quad \boldsymbol{\eta}_i \sim N_K(0, I), \quad \boldsymbol{\epsilon}_i \sim N_P(0, \Sigma_0), \\ \Sigma_0 &= \text{diag}(\sigma_1^2, \dots, \sigma_P^2) \\ i &= 1, \dots, N. \end{aligned}$$

The prior induced on the latent  $\mathbf{z}_i$  by integrating out the unknown  $\boldsymbol{\eta}_i$  is then:

$$(2) \quad \mathbf{z}_i \sim N(0, \Lambda \Lambda' + \Sigma_0),$$

yielding a lower dimensional representation of the covariance between measurements.

**Chemical features are often non-normal (e.g. count, skewed continuous, or binary).** Many chemical descriptors from Mold2 are counts of particular elements (number of carbon, number of oxygen, etc.).

In order to allow this framework to encompass data of mixed type, define:

$$(3) \quad x_{is} = f_s(z_{is}), \quad i = 1, \dots, N, \quad s = 1, \dots, S.$$

The particular link function  $f_s$  depends on the feature specification, allowing for mixed scale data via selection of an appropriate link by scale and type. Let  $f_s(z_{is}) = z_{is}$  or  $f_s(z_{is}) = \log(z_{is})$  for continuous  $x_{is}$ , with the latter chosen for strictly positive and positively skewed cases. Let  $f_s(z_{is}) = 1(z_{is} > 0)$  for binary  $x_{is}$ , where  $1(\cdot)$  is an indicator function taking the value of 1 when the argument is true and 0 when the argument is false. Categorical variables may be incorporated under this framework by transforming the  $C$  categories into  $C - 1$  binary variables indicating whether or not the categorical value for that individual took a given non-baseline category value; the result is that either none or one of the  $C - 1$  variables will take on a value of 1. Finally for count  $x_{is}$ , which may or may not be zero-inflated, let  $f_s(z_{is})$  be a rounding operator such that  $f_s(z_{is}) = 0$  if  $z_{is} < 0$  and  $f_s(z_{is}) = t$  if  $t - 1 \leq z_{is} < t$ , as specified in (Canale and Dunson, 2013).

**There is likely a shared low dimensional space underlying chemical features and activity.** BS<sup>3</sup>FA assumes that some underlying factors explain all of the variation in the dose response curves and, jointly, part of the variation in the associated chemical features. Recall  $\mathbf{z}_i$  and  $\mathbf{y}_i$  denote  $S$ - and  $D$ -dimensional (latent) continuous features and observed dose response curves, respectively, for observation  $i$ . Assume each is mean centered and that the indexing of  $\mathbf{y}_i$  is such that the function is ‘in order’ (for the ToxCast data, in order means that the  $D$  unique doses are sorted such that the doses increase with index). Also, for notational convenience assume that functional data  $\mathbf{y}_i$  are only observed once per index (the case of notationally awkward multiply observed doses is explicitly addressed in the Gibbs sampler described in the Appendix). BS<sup>3</sup>FA models

$$(4) \quad \begin{aligned} \mathbf{z}_i &= \underset{S \times 1}{\Theta} \underset{S \times K}{\boldsymbol{\eta}_i} + \underset{S \times J}{\Xi} \underset{J \times 1}{\boldsymbol{\nu}_i} + \underset{S \times 1}{\mathbf{e}_i}, \\ \mathbf{y}_i &= \underset{D \times 1}{\Lambda} \underset{D \times K}{\boldsymbol{\eta}_i} + \underset{D \times 1}{\boldsymbol{\epsilon}_i}, \\ i &= 1, \dots, N. \end{aligned}$$

The form of the above model is that of a set of linked factor models. Note that although there are three non-error component pieces (namely  $\Theta \boldsymbol{\eta}_i$ ,  $\Xi \boldsymbol{\nu}_i$ , and  $\Lambda \boldsymbol{\eta}_i$ ), there are only two unique factor vectors:  $\boldsymbol{\eta}_i$  and  $\boldsymbol{\nu}_i$ . These factors are highly interpretable. The term  $\boldsymbol{\eta}_i$  represents the shared latent



space underlying structured variability in both  $\mathbf{z}_i$  and  $\mathbf{y}_i$  (note that it appears in both factor models). In the expression for  $\mathbf{y}_i$  it is the sole factor vector and in that for  $\mathbf{z}_i$  it is one of two factor vectors. Thus, it is responsible for all structured variation in  $\mathbf{y}_i$  but only part of the structured variation in  $\mathbf{z}_i$ . The term  $\boldsymbol{\nu}_i$  represents structured variation in  $\mathbf{z}_i$  that is *unrelated* to  $\mathbf{y}_i$ .

In the above model, the mean of  $\mathbf{z}_i$  is  $\Theta\boldsymbol{\eta}_i + \Xi\boldsymbol{\nu}_i$ , and  $\mathbf{e}_i$  is a term for unstructured noise in  $\mathbf{z}_i$ . Similarly, the mean of  $\mathbf{y}_i$  is  $\Lambda\boldsymbol{\eta}_i$ , and  $\boldsymbol{\epsilon}_i$  is the unstructured noise term for  $\mathbf{y}_i$ . The priors on the shared factors  $\{\boldsymbol{\eta}_i\}$ , the  $X$ -specific factors  $\{\boldsymbol{\nu}_i\}$ , and error terms are set to be those typically used in factor analysis:

$$(5) \quad \begin{aligned} \boldsymbol{\eta}_i &\sim N_K(0, I), & \boldsymbol{\nu}_i &\sim N_J(0, I), \\ \mathbf{e}_i &\sim N_S(0, \Sigma_X), & \Sigma_X &= \text{diag}(\sigma_{X,1}^2, \dots, \sigma_{X,S}^2), \\ \boldsymbol{\epsilon}_i &\sim N_D(0, \Sigma_Y), & \Sigma_Y &= \text{diag}(\sigma_Y^2, \dots, \sigma_Y^2), \end{aligned}$$

Homoscedastic variance is assumed for dose-response curves  $Y$ . Fix  $\sigma_{X,s}^2$  to 1 if feature  $s$  is binary, for reasons of identifiability.

Note that as of yet, we have not discussed the functional nature of the  $\mathbf{y}_i$ , nor the issue of many entries in  $\mathbf{z}_i$  likely being unrelated to  $\mathbf{y}_i$ . The following sections will describe how structure can be imposed on  $\Lambda$  and  $\Theta$ , respectively, in light of these considerations.

**The dose-response curve data are functional in nature.** Figure 2 shows the noisy observations from a set of example chemicals, but the underlying signal represents a smooth curve relating chemical dose to response.

For functional data it is preferable to have each loading vector (i.e., each column of  $\Lambda$ ) itself be functional. The desired smoothness of the mean curves underlying noisy observations  $\mathbf{y}_i$  can thus be imposed via the choice of smooth priors on the loading matrix  $\Lambda$ . Let  $\boldsymbol{\lambda}_k$  denote the  $k$ th column of  $\Lambda$ , so

$$\Lambda = \begin{bmatrix} | & | & \dots & | \\ \boldsymbol{\lambda}_1 & \boldsymbol{\lambda}_2 & \dots & \boldsymbol{\lambda}_K \\ | & | & & | \end{bmatrix}.$$

In order to learn rather than prescribe smooth bases, columns of  $\Lambda$  are modeled as  $D$ -dimensional Gaussian processes:

$$(6) \quad \boldsymbol{\lambda}_k \sim \mathcal{GP}(0, c_k(\cdot)), \quad c_k(d, d') = \alpha_k^2 e^{-\frac{(d-d')^2}{2\ell^2}}, \quad k = 1, \dots, K.$$

The Gaussian process function variance  $\alpha_k^2$  is comprised of two components: a global inverse variance term  $\phi$  and a column-specific inverse variance term  $\tau_k$ . The column-specific inverse variance term  $\tau_k$  utilizes the multiplicative gamma process prior of (Bhattacharya and Dunson, 2011), leading to stochastic shrinkage of columns of  $\Lambda$  toward 0 by index.

$$(7) \quad \begin{aligned} \alpha_k^2 &= (\phi\tau_k)^{-1}, & \tau_k &= \prod_{h=1}^k \delta_h, & k &= 1, \dots, K, \\ \phi &\sim \text{Ga}(g_\phi/2, g_\phi/2), & \delta_1 &\sim \text{Ga}(a_1, 1), & \delta_h &\sim \text{Ga}(a_2, 1), & h &\geq 2. \end{aligned}$$

Following the note by (Durante, 2017) on hyperparameter selection, set  $a_1 = 2.1$  and  $a_2 = 3.1$  in equation (7). The value of  $g_\phi$ , the hyperparameter for the global function precision of the GP, should be chosen to reflect the scale of the data.

This stochastic shrinkage leads to an effective truncation of the factors and an automatically learned dimension of the latent space so long as  $K$  is chosen large enough (whether  $K$  is adequately large can be assessed by monitoring the convergence of  $\alpha_k^2$  to 0 as  $k$  approaches  $K$ ). To see why, consider the model for  $\mathbf{y}_i$  written in expanded form:  $\mathbf{y}_i = \boldsymbol{\lambda}_1 \eta_{i,1} + \boldsymbol{\lambda}_2 \eta_{i,2} + \dots + \boldsymbol{\lambda}_K \eta_{i,K} + \boldsymbol{\epsilon}_i$ . Assuming  $K$  is large enough, as  $k$  approaches  $K$ , the vector  $\boldsymbol{\lambda}_k$  should be approximately the 0-vector, meaning that many of the later terms will contribute negligibly to the mean of  $\mathbf{y}_i$ . See Figure 7 for a visualization of  $\Lambda$  and column shrinkage.

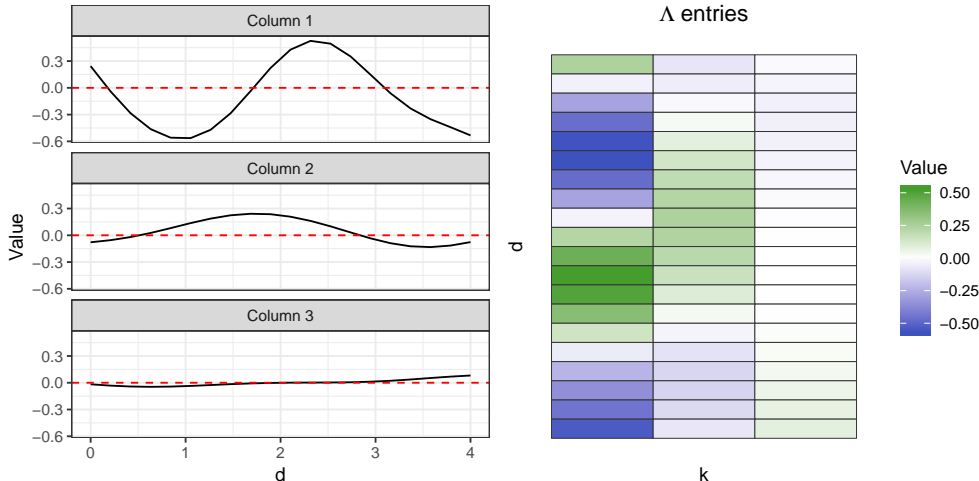


Fig 7: Visualization of the smoothness and the shrinkage of columns of an example  $D = 20$  by  $K = 3$  loadings matrix  $\Lambda$ . The effect is an automatic truncation of the number of factors in the model and a learned latent dimension. In this figure columns of  $\Lambda$  were sampled using the kernel in equation (6) with  $\ell^2 = 1$  and  $\alpha_k^2$  being 1,  $\frac{1}{25}$ ,  $\frac{1}{400}$  for  $k = 1, 2, 3$ , and the indices  $d$  corresponding to the length-20 vector from 0 to 4, inclusive. Note that as  $\alpha_k^2$  decreases, the functions tend to flatten.

**Many features are likely unimportant for certain aspects of chemical activity.** That is, if a set of chemical descriptors has not been carefully selected to be toxicity-relevant, it is unlikely that all are related to the shape of the dose-response curves. Even if all features are toxicity-relevant, it is plausible that features will impact different pieces of the toxicity profile (e.g., some features may impact the steepness of the dose-response, while others may impact the height of the final plateau). The way to encourage such a relationship is via element-wise shrinkage, i.e. zeros in entries, of the factor loadings matrix  $\Theta$ .

Shrinkage on elements  $\theta_{sk}$  of  $\Theta$  is desirable because it is likely that for a given factor many features have negligible impacts on the associated component of the functional  $\mathbf{y}_i$ . Explicitly,

$$\Theta = \begin{bmatrix} \theta_{11} & \theta_{12} & \theta_{13} & \dots & \theta_{1K} \\ \theta_{21} & \theta_{22} & \theta_{23} & \dots & \theta_{2K} \\ \vdots & \vdots & \vdots & \ddots & \vdots \\ \theta_{S1} & \theta_{S2} & \theta_{S3} & \dots & \theta_{SK} \end{bmatrix}$$

There is a very rich literature proposing elaborate shrinkage and sparsity priors for factor loadings (e.g., (Yoshida and West, 2010; Meng et al., 2010; Knowles et al., 2011; Pati et al., 2014)). We opt for a horseshoe prior (Carvalho, Polson and Scott, 2010) modified for simple sampling (Makalic

and Schmidt, 2016) on entries  $\theta_{sk}$  of  $\Theta$ :

$$\begin{aligned}
 \theta_{sk} &\sim \text{N}(0, \beta^2 \gamma_{sk}^2 \tau_k^{-1}), \\
 \beta^2 | t &\sim \text{IG}(1/2, 1/t) \\
 \gamma_{sk}^2 | b_{sk} &\sim \text{IG}(1/2, 1/b_{sk}) \\
 \{b_{sk}\}, t &\sim \text{IG}(1/2, 1), \\
 s &= 1, \dots, S, \quad k = 1, \dots, K.
 \end{aligned}
 \tag{8}$$

The horseshoe component of this prior is in the hierarchical hyper-prior on global variance term  $\beta^2$  and local variance term  $\gamma_{sk}^2$ . The column-specific variance  $\tau_k^{-1}$  applies stochastically increasing shrinkage as column index increases. See Figure 8 for a visualization of  $\Theta$  and column shrinkage.

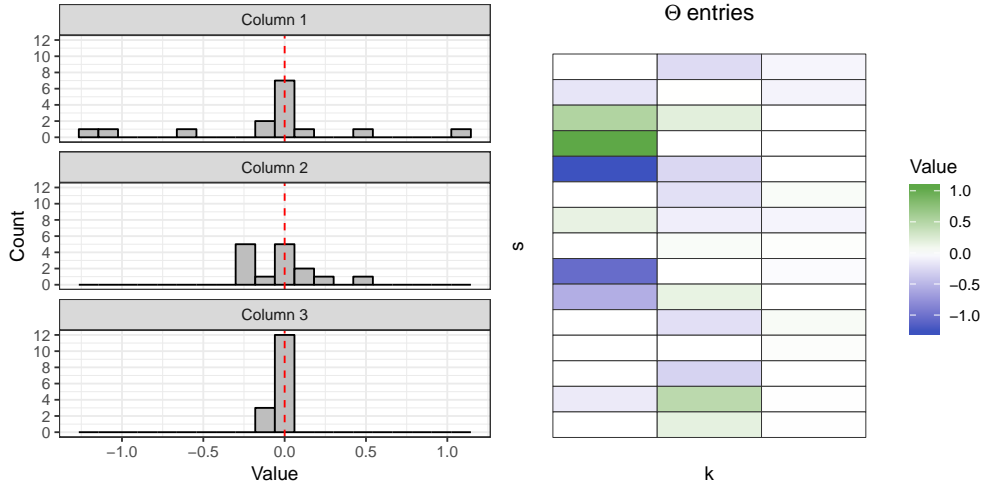


Fig 8: Visualization of elementwise sparsity and the shrinkage of columns of an example  $S = 15$  by  $K = 3$  loadings matrix  $\Theta$ . The effect is an automatic truncation of the number of factors in the model and a learned latent dimension. In this figure columns of  $\Theta$  had column-specific variance  $\tau_k^{-1}$  being  $1, \frac{1}{25}, \frac{1}{400}$  for  $k = 1, 2, 3$ .

**The dimension of the latent space underlying the dose response curves and of that underlying toxicity-relevant features should be the same.**

The same column-specific precision  $\tau_k^{-1}$  is used for both  $\Theta$  and  $\Lambda$ , so relative column shrinkage is applied consistently across the two matrices. The result is the same effective truncation on the number of latent factors in the joint space. This specification, along with the common  $\eta_i$ , is what allows the shared directions of variability between  $\mathbf{y}_i$  and  $\mathbf{x}_i$  to be learned. Distance can be defined over the  $\boldsymbol{\eta}$ -vector with elements  $\eta_k$  weighted by precision  $\tau_k^{-1}$ , to give a sense of closeness in “ $\boldsymbol{\eta}$  space” that reflects the true amount of information contained in each latent direction.

**There is additional variability in chemical structure beyond that which impacts chemical activity.** Unless all chemical features were carefully hand-selected to be toxicity relevant for the specific assay considered in the model (a tall task, and unlikely to be completely true no matter how careful the selection), accounting for variability in  $\mathbf{z}_i$  shared with  $\mathbf{y}_i$  will not capture all structured variability in chemical features.

After accounting for the variability in  $\mathbf{z}_i$  shared with  $\mathbf{y}_i$  (via latent factor  $\boldsymbol{\eta}_i$ ),  $\mathbf{z}_i$  may still have structured variation due to individual latent factor  $\boldsymbol{\nu}_i$ . Let  $\mathbf{z}_i^* = \mathbf{z}_i - \Theta \boldsymbol{\eta}_i$ . Then  $\mathbf{z}_i^* = \Xi \boldsymbol{\nu}_i + \mathbf{e}_i$ , which

once again looks like a traditional factor model. The direct application of priors in (Bhattacharya and Dunson, 2011) is used for elements of  $\Xi$ . Specifically elements  $\xi_{s,j}$  of  $\Xi$  are given prior

$$(9) \quad \begin{aligned} \xi_{s,j} | \kappa_{sj}, \omega_j &\sim N(0, \kappa_{sj}^{-1} \omega_j^{-1}), \quad \omega_j = \prod_{h=1}^j \zeta_h, \quad s = 1, \dots, S, \quad j = 1, \dots, J, \\ \kappa_{sj} &\sim \text{Ga}(g_\kappa/2, g_\kappa/2), \quad \zeta_1 \sim \text{Ga}(m_1, 1), \quad \zeta_h \sim \text{Ga}(m_2, 1), h \geq 2. \end{aligned}$$

Stochastic column-specific shrinkage via the  $\omega_j^{-1}$  term removes the need to select an ideal number of factors  $J$  and allows for simply selecting  $J$  “large enough.” This formulation also allows for efficient Gibbs sampling of the posterior. Following the note by (Durante, 2017) on hyperparameter selection, set  $m_1 = 2.1$  and  $m_2 = 3.1$  in equation (9). The value of  $g_\kappa$ , the hyperparameter for the entry-level precision terms of  $\Xi$ , should be chosen to reflect the scale of the data.

If there is in fact no additional variability in  $\mathbf{z}_i$  beyond that shared with  $\mathbf{y}_i$ , the following specification allows for all columns of  $\Xi$  to be shrunk to 0-vectors. This case reduces to a fully joint factor model in which all variability in  $\mathbf{z}_i$  is shared with  $\mathbf{y}_i$ .

**Chemical activity is not necessarily measured on a fully observed, regularly spaced grid.** There are a handful of common dose measurements at which the majority of chemicals are measured (see Figure 11), but there are many chemicals whose observations are less regular. Furthermore, some chemicals have multiple observed dose response curves.

The issue of irregular spacing between the unique values associated with the indices is handled automatically via the use of GPs for modeling columns of  $\Lambda$ . The covariance between points is defined by the kernel for any pair of input values (see equation (6)) and not dependent on a regular measurement grid.

**Toxicologists may wish to report different components and/or summaries of predicted dose-response curves.** For example, they may be interested in the dose value at which the response first exceeds some threshold, the maximum response value reached, the area under the curve, etc. Each of these summaries provides different information about the dose response relationship. An advantage of a Bayesian formulation is that we can obtain posterior samples for any functional of the dose response curve trivially, with these samples then used to obtain point and interval estimates.

**3.2. Posterior computation.** The posterior for the BS<sup>3</sup>FA model is not available in closed form. However, closed form full conditional distributions of the parameters associated with the model allow the use of a straightforward Gibbs sampler for these draws. Samples obtained directly from this Markov chain Monte Carlo (MCMC) algorithm allow for the calculation of posterior means and credible intervals for identifiable model components, including the predicted mean, covariance, and noise variance of  $X$  and  $Y$ . A post-processing step to resolve rotational ambiguity and account for label/sign switching allows for identifiability of the individual model components, including the factor scores  $\eta$  and loadings  $\Lambda$  and  $\Theta$  (code modified from [https://github.com/poworoznek/sparse\\_bayesian\\_infinite\\_factor\\_models](https://github.com/poworoznek/sparse_bayesian_infinite_factor_models)). Full details on the Gibbs sampler steps and initialization are included in the Supplemental Materials.

**3.3. Code base and reproducibility.** Code for simulating data and sampling from the BS<sup>3</sup>FA model, along with a user manual, are made available at <https://github.com/kelrenmor/bs3fa>. A hands-on demonstration of the package is available at <https://www.youtube.com/watch?v=qLyxBQ->

**sVcY**. Code specific to this paper (i.e., to reproduce the simulations, figures, and results) is provided in the online supplementary material.

**3.4. Simulation study.** Simulation studies were performed in order to assess the ability of BS<sup>3</sup>FA to learn the true toxicity-relevant distance between chemicals, its predictive performance, and the model fit. Two broad categories of simulations were performed: first, those in which the true data generating process aligns with model assumptions (i.e., when data are simulated from a partially shared latent factor model) and when it does not (i.e., when data are simulated from something other than a factor model). In the former category, we also assess how well model sub-components can be learned.

For all simulations, 25% of simulated “chemicals” are held out. That is, rather than withholding 25% of dose-response observations across chemicals, we withhold all dose-response data for each hold-out chemical. For distance performance, BS<sup>3</sup>FA is compared to Euclidean distance using all features, PCA, and Euclidean distance using the features having coefficients whose 95% credible intervals don’t span 0 in the Bayesian function-on-scalars regression (B-FOSR) of (Kowal and Bourgeois, 2018). For predictive performance, BS<sup>3</sup>FA is compared to the BAABTP model (Wheeler, 2019), B-FOSR, and least absolute shrinkage and selection operator (LASSO) using each covariate, dose, and all pairwise interactions. We attempted to also compare the MSPE of a frequentist FOSR using the **refund** package in **R**, but the **fosr.vs()** function returned an error saying the dimension of  $\mathbf{y}_i$  was not high enough relative to  $\mathbf{x}_i$  (i.e., that  $D$  was too small relative to  $S$ ).

For simulations in which the true data generating process aligns with model assumptions, the true dimension of the latent toxicity-relevant space  $K$  was varied, taking values 1, 3, and 5. For each  $K$ , the true dimension of the latent toxicity-irrelevant space  $J$  was varied from 0 to 20 in intervals of 5. At each combination of  $K$  and  $J$ , 100 data sets were simulated with  $N = 300$ ,  $D = 10$ ,  $S = 40$ . For roughly half of the chemicals in each data set,  $\boldsymbol{\eta}_i$  was set to a zero vector for that chemical (i.e., for each simulated data set, there was a 50% chance that any given chemical was non-activating). Further simulation details are provided in the Supplemental Materials. Overall, the model does quite well at capturing the structure of the noise variance and the true components  $\Lambda$  and  $\Theta$ .

Figure 9 shows the correlation between entries in the true pairwise distance matrix (i.e., the Euclidean distance between true latent factors  $\boldsymbol{\eta}$ ) and the predicted pairwise distance matrix for holdout chemicals. We see that even in the case of small  $J$ , performing PCA on the  $S$ -dimensional  $X$  matrix obscures the true distance in the latent space. As  $J$  increases, the correlation between the chemical distance in the true  $\boldsymbol{\eta}$  and that in either PCA space or Euclidean space drops quickly. The BS<sup>3</sup>FA has stable high correlation across all values of  $J$  and  $K$ .

Figure 10 shows the mean squared predictive error (MSPE) for the simulated hold-out chemicals’ dose-response mean functions. Although the performance of all models deteriorates as the amount of “superfluous” information in  $X$  increases (i.e., as  $J$  increases), the BS<sup>3</sup>FA model is the most robust, showing superior performance across all values of  $K$  and  $J$ . The BAABTP model appears most sensitive to the value of  $J$ , with MSPE near that of BS<sup>3</sup>FA model when  $J$  is small, but among the worst MSPE when  $J$  is high. The LASSO model is able to perform fairly well when  $K$  is small, but as  $K$  increases it is unable to learn the more complicated relationship between  $\mathbf{x}_i$  and  $\mathbf{y}_i$ . The B-FOSR model exhibited unstable predictions for hold-out chemicals, leading to MSPEs far above the visual display range shown in the figure. Thus, those results are omitted.

Pointwise coverage of the BS<sup>3</sup>FA model (shown in detail in the Supplemental Materials) remains close to nominal across all values of  $K$  and  $J$ . The coverage of the BAABTP model decreases as  $J$

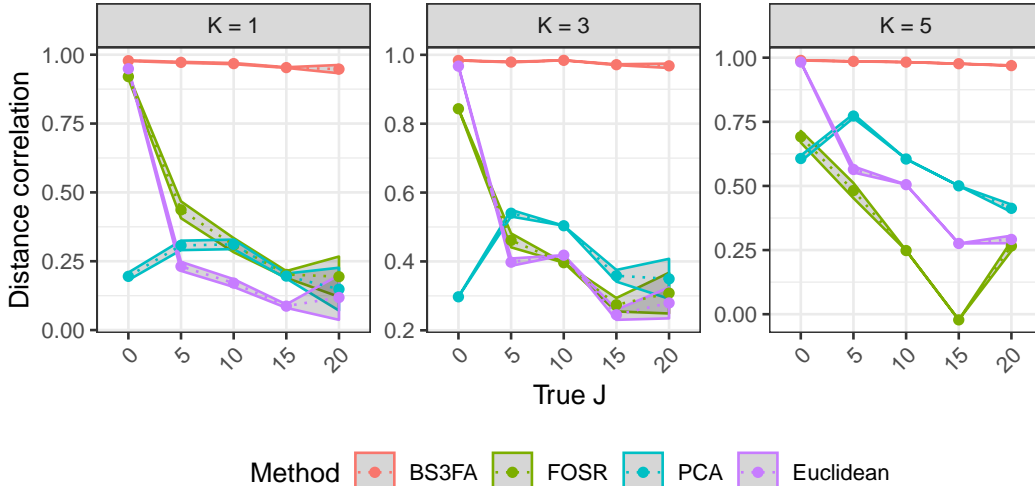


Fig 9: Correlation between entries in the true pairwise distance matrix (i.e., the Euclidean distance between true latent factors  $\eta$ ) and the predicted pairwise distance matrix for holdout chemicals. Each subplot shows the result of 100 simulations per  $J$  across methods for a given true shared subspace dimension  $K$ .

increases, another reflection of its overall poor predictive performance.

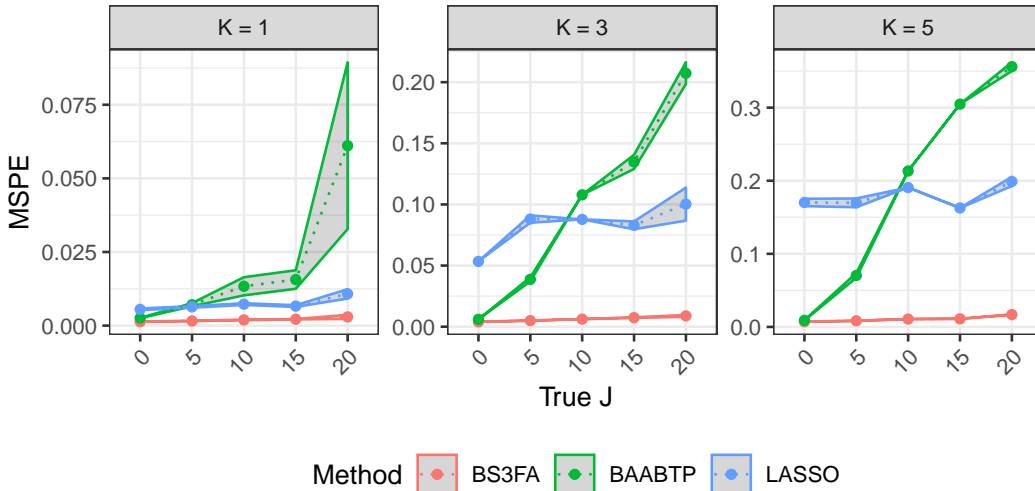


Fig 10: Mean squared predictive error (MSPE) for the hold-out chemicals' dose-response mean functions. Each subplot shows the result of 100 simulations per  $J$  across methods for a given true shared subspace dimension  $K$ .

In the ToxCast analysis following this section, we discuss results from one possible method of deeming a chemical “activity increasing,” i.e. activating. Namely, call a chemical activating if its 95% credible interval for predicted dose response profile exceeds 0 at any point. Note that for other assays activity suppression may also be of interest, and in these cases the definition of activity could be relaxed to require that the credible interval does not contain zero at some point. The true positive rate (TPR), false positive rate (FPR), and false discovery rate (FDR) of this method on the simulated data are shown in Table 1. Across all values of  $K$  and  $J$  the TPR is generally high, and the FPR and FDR are fairly low. Note that the TPR, FPR, and FDR increase with  $K$ , while the TPR decreases with  $J$ . That is, the model seems more likely to identify chemicals as activating

as the dimension of the latent toxicity-relevant space increases, but loses sensitivity when there is more toxicity-irrelevant information.

		$J = 0$	$J = 5$	$J = 10$	$J = 15$	$J = 20$
TPR	$K = 1$	0.80 (0.07)	0.76 (0.07)	0.73 (0.08)	0.70 (0.04)	0.67 (0.03)
	$K = 3$	0.97 (0.00)	0.98 (0.01)	1.00 (0.00)	0.98 (0.02)	0.97 (0.03)
	$K = 5$	1.00 (0.00)	1.00 (0.00)	1.00 (0.00)	1.00 (0.00)	1.00 (0.01)
FPR	$K = 1$	0.02 (0.02)	0.02 (0.03)	0.02 (0.02)	0.03 (0.01)	0.01 (0.01)
	$K = 3$	0.05 (0.00)	0.06 (0.01)	0.05 (0.00)	0.05 (0.04)	0.02 (0.03)
	$K = 5$	0.09 (0.05)	0.09 (0.05)	0.14 (0.01)	0.09 (0.02)	0.05 (0.04)
FDR	$K = 1$	0.02 (0.03)	0.03 (0.04)	0.03 (0.03)	0.03 (0.01)	0.02 (0.02)
	$K = 3$	0.05 (0.00)	0.04 (0.02)	0.05 (0.00)	0.05 (0.04)	0.02 (0.02)
	$K = 5$	0.08 (0.05)	0.08 (0.05)	0.12 (0.01)	0.06 (0.02)	0.05 (0.03)

Table 1: True positive rate (TPR), false positive rate (FPR), and false discovery rate (FDR) for the proposed method of assessing whether a chemical is activating. A perfect classifier has a TPR of 1 and an FPR/FDR of 0.

When there is misalignment between the structure assumed by the BS<sup>3</sup>FA model and the true data generating process, BS<sup>3</sup>FA is still able to predict similarly to or better than the two highest performing competitors: BAATP and LASSO. As with the well-aligned simulation, BS<sup>3</sup>FA is robust to increasing “superfluous” information in  $X$ . A similar story can be seen in the coverage and distance results for the misaligned simulation. Even when the assumed latent factor model is not the model from which data are simulated, the coverage of BS<sup>3</sup>FA is close to nominal. BAABTP, on the other hand, suffers from much lower-than nominal coverage as “superfluous” information in  $X$  increases. BS<sup>3</sup>FA is still able to recover a distance metric that is highly correlated with the distance in the true relevant  $X$  dimensions. Visual results are shown in the Supplemental Materials.

**4. Relating chemical structure to toxicological response.** Data pre-processing steps and results of the analysis of the ToxCast ATG PXR assay are discussed in the following subsections. The structure of BS<sup>3</sup>FA allows for learning about structured variability in both the feature and response space, prioritizing chemicals for future evaluation, and predicting chemical activity for as-yet-unobserved chemicals.

**4.1. ToxCast setup.** Observations below the cytotoxicity limit for 3540 Phase 1, Phase 2, and e1k chemicals tested in the AttaGene PXR assay are included in our data analysis. The structure information for each chemical is summarized by 777 Mold2 chemical features (Hong et al., 2008). As discussed previously, BS<sup>3</sup>FA has the advantage of being able to effectively ignore toxicity-irrelevant features via shrinkage on elements of  $\Theta$ , making the careful curation of a feature set unnecessary.

Chemicals having no provided SMILES information ( $n = 405$ ) were omitted from further analysis. The result is 3135 chemicals having Mold2 descriptions of their chemical structure. Note that some chemicals have identical Mold2 output. These sets of chemicals are in effect considered a single chemical (i.e., treated as multiply observed dose response curves by the model). For analysis the number of ‘unique’ chemical sets (i.e. the number of unique SMILES represented across the 3135 chemicals) is  $N = 3070$ . The 8 most common dose concentrations are -1.05, -0.52, -0.1, 0.3, 0.85, 1.3, 1.85, 2.3 log uM (see the vertical white bands in Figure 11), but BS<sup>3</sup>FA allows both common



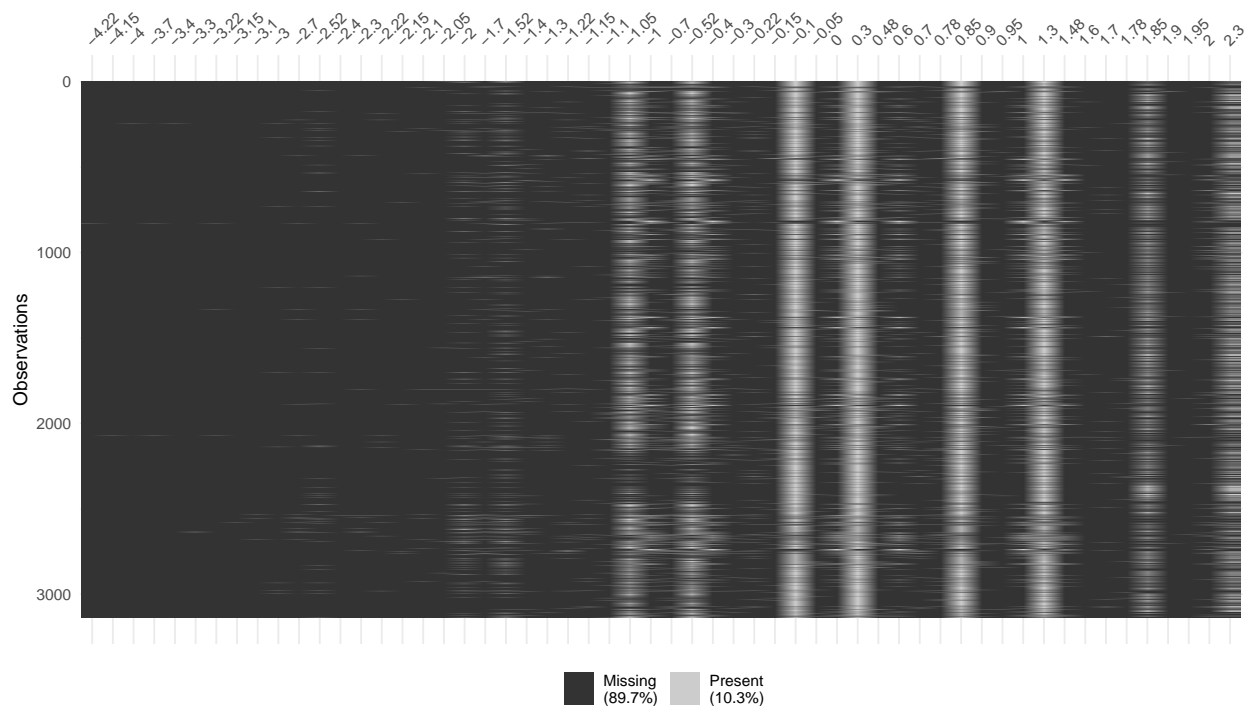


Fig 11: Missingness by dose for each chemical in the analysis. Each row corresponds to a chemical, and each column to a dose value (sorted in ascending order). Note that very few chemicals have observations below  $-2 \log \text{uM}$ .

and unique doses. As the bulk of chemicals have no information about extremely low ( $< -2 \log \text{uM}$ ) dose activity (see Figure 11), the data considered are the  $D = 38$  unique doses  $\geq -2 \log \text{uM}$ , out of the 56 total unique doses. Approximately 4% of chemicals have multiply observed dose response curves, e.g. Allethrin and Clorophene from Figure 2.

Mold2 is used to generate a set of 777 numeric molecular descriptors associated with each chemical. As noted above, some chemicals exactly shared these descriptors due to Mold2’s inability to capture certain differentiating structures (see the Supplemental Materials for an example); these “identical” chemicals were treated as multiply observed chemicals. After removing features having no variability (99 total, including, e.g., features equalling 0 for all chemicals such as number of 11-membered rings and number of Argon), features with duplicated entries (16), or features having  $> 99\%$  of chemicals sharing a feature value (99, e.g. only one chemical has any aromatic group urea derivatives),  $S = 563$  features remain. As a further pre-processing step, the variables are scaled to have mean 0 and variance 1. Further information on creating and using Mold2 descriptors is included in the Supplemental Materials.

In order to mimic the scenario of using the BS<sup>3</sup>FA model to prioritize chemicals for further screening, we hold out all of the dose-response observations for 25% of chemicals in the data set. That is, we provide the model with these chemicals’ structure but not their dose-response curves. Of interest will be how similar these unobserved chemicals are to known activating chemicals, and the AC50 (the dose at 50% of maximum activity) for unobserved chemicals predicted by the model to be activating. For the purpose of this analysis, we consider a chemical activating if the lower bound of its 95% posterior credible interval for the expected dose response curve ever exceeds 0.

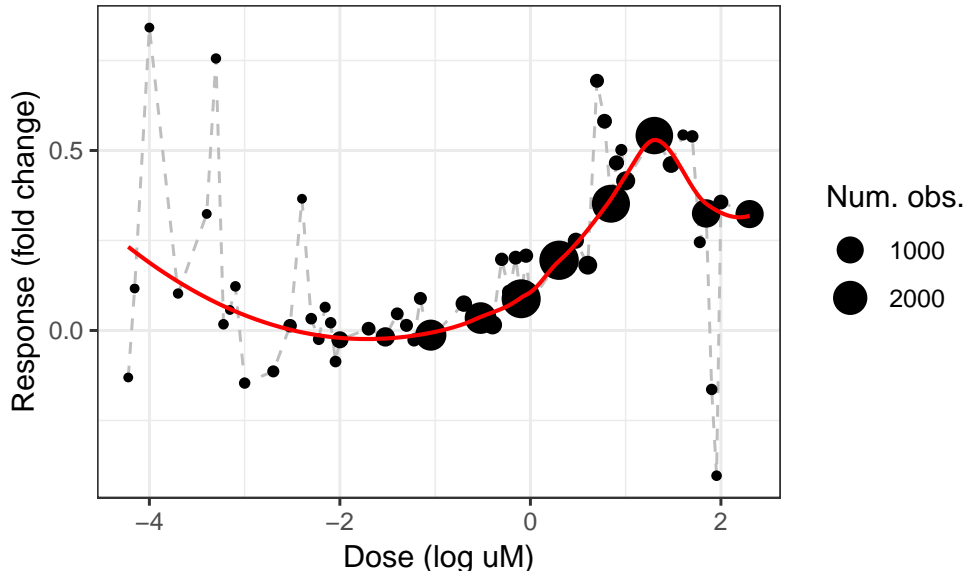


Fig 12: Average response value at each dose in the data set (solid dots) with size proportional to the number of observations at that dose. The dashed (grey) line shows the result of connecting each of these dose-specific averages, whereas the solid (red) line shows the average dose response curve found via LOESS (locally weighted smoothing), with settings discussed in the Supplemental Materials. The latter is the mean curve used to center the dose response curves in the analysis.

The low number of observations at less common doses leads to a ‘noisy’ estimate of the average dose response curve (see the dashed grey line in Figure 12). LOESS smoothing creates a functional mean curve that can be subtracted from each observation prior to model fitting, a data cleaning step to reflect the assumption that the GPs on columns of  $\Lambda$  are centered at 0 (this correction is added back in after model fitting prior to assessing whether the lower credible interval is positive at any dose). Additionally, both the structure and the dose-response matrices are scaled by their Frobenius norms so that the scaled matrices have the same Frobenius norm (a measure of total variation); specifically set  $X = c \frac{X}{\|X\|_F}$  and  $Y = c \frac{Y}{\|Y\|_F}$ , with  $c$  some constant chosen large enough to keep the shrinkage priors on the loadings matrices meaningful. This rescaling keeps larger matrices from dominating when learning the shared column-specific shrinkage terms  $\{\tau_k\}$  or the shared score vectors  $\{\eta_i\}$  (e.g., when  $S$  is much larger than  $D$ , as in this setting).

We ran the sampler for 40,000 iterations. After an initial burn-in of 20,000 iterations, every 10th sample was saved. Computation time was approximately 8 hours on a 2016 MacBook pro with a 2.9 GHz Intel Core i7 processor. Trace plots of model predictions show good mixing; these, along with those of model components and an assessment of the sufficiency of the chosen  $K$  and  $J$  values, are available in the Supplemental Materials.

**4.2. Model components.** The learned matrix  $\Lambda$ , shown on the left side of Figure 13, provides a snapshot of the directions of structured variation present in the dose-response data. The first column of  $\Lambda$ , shown in the top middle of Figure 13, is the dominant factor loading (i.e., the factor loading having the largest estimated norm). Unsurprisingly, this vector takes the shape of a prototypical dose response curve. Later columns of  $\Lambda$  act to provide smooth deviations from this prototypical shape. For example, the second column characterizes a close to linear increase until leveling off at a dose value just under 2 log uM, while the fourth column shows an initial dip below zero.

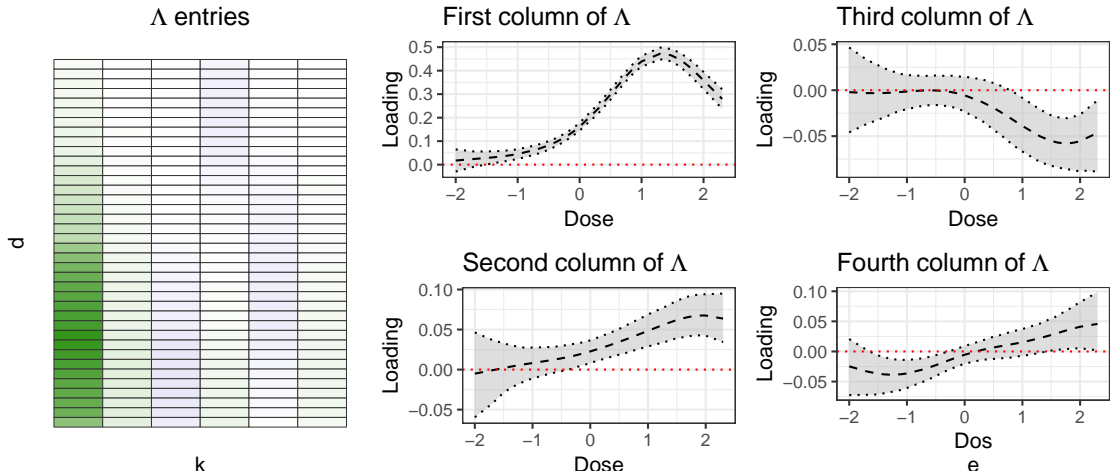


Fig 13: Left: First 6 columns of the predicted mean of  $\Lambda$ . Each row represents a unique dose value. Middle and right: Mean and 95% credible intervals for the first four columns of  $\Lambda$ . The dose values are given on the  $x$ -axis.

The learned matrix  $\Theta$ , the values of which are shown in Figure 14, provides a snapshot of the directions of structured toxicity-relevant variation present in the feature data. The bulk of the estimated entries are very close to 0 due to the shrinkage effect of the horseshoe prior. The BS<sup>3</sup>FA model structure allows us to interpret the nonzero entries of a given column of  $\Theta$  as being those related to the particular structure present in the corresponding column of  $\Lambda$ . For example, the significantly non-zero entries of the first column of  $\Theta$  are those associated with the prototypical activity profile seen in the top right of Figure 13. By absolute magnitude, the largest such features include the number of group X-C on aromatic ring, molecular regression coefficients surface LogP index, sum eigenvalue weighted by van der Waals distance matrix, sum of topological distance between the vertices O and Cl, and number of Chlorine.

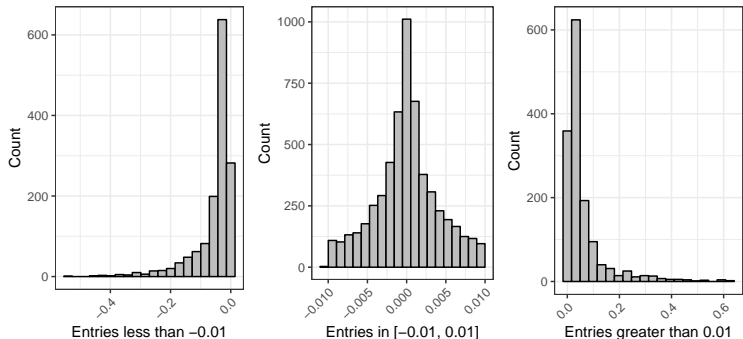


Fig 14: Histogram showing entries of the predicted mean of  $\Theta$ . The bulk of the estimated entries are close to 0 due to the shrinkage effect of the horseshoe prior.

The chemicals having extreme positive values of  $\eta_1$  will be those for which the dose-response profile has a large component due to  $\lambda_1$  and a large chunk of toxicity-relevant molecular variability described by the first column of  $\Theta$ . In the training set, the chemicals having the largest expected value for  $\eta_1$  are Mercuric chloride, Benzyltriphenylphosphonium chloride, Sodium chlorite, 1,1-Bis(3-cyclohexyl-4-hydroxyphenyl)cyclohexane, and Basic Blue 7. All but 1,1-Bis(3-cyclohexyl-4-hydroxyphenyl)cyclohexane, which is a known irritant, are known toxins. These chemicals all have in common the presence of Cl, so it is unsurprising that features involving Cl appeared amongst

the high-value loadings components for the first column of  $\Theta$ .

**4.3. Distance learning.** Figure 15 shows the predicted pairwise distance matrix between a set of example chemicals, chosen as clusters of chemicals in the training set closest to specific recognizable hold-out chemicals. Included are a cluster of similar low-activity chemicals (the training chemicals nearest to hold-out chemical Acetaminophen) in the bottom left block, and a cluster of similar high-activity chemicals (the training chemicals nearest to hold-out chemical Bisphenol B, which include Bisphenol A) in the central block. A handful of miscellaneous chemicals that are fairly isolated in  $\eta$  space relative to the other included chemicals are shown in the top right block.

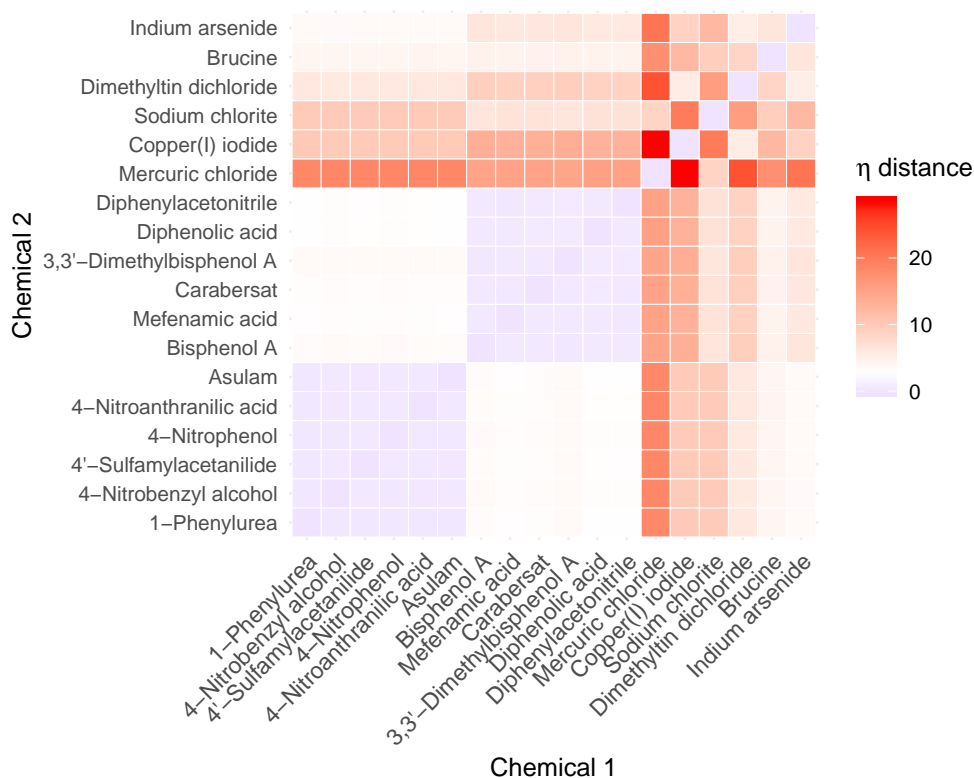


Fig 15: Expected distance in  $\eta$  space for a select set of training chemicals.

When selecting future chemicals for prioritization, one can either seek to “fill in” the space around chemicals of known toxicity relevance, or to “venture out” into spaces not near any currently tested chemicals. While addressing this experimental design problem is outside the scope of this work, we assume for the sake of exposition that both possible avenues are of interest. We further assume that the set of hold-out chemicals represents the space of options for further *in vitro* testing.

Assuming the central cluster of chemicals in Figure 15 is of interest for more targeted exploration, we could select the hold-out chemicals closest to that set to test further. In terms of average distance between each cluster member, the three closest chemicals in the hold-out set are Bisphenol B (i.e., our ‘seed’ chemical for this training group), Phenytoin, and 2,5-Bis(2-methylbutan-2-yl)benzene-1,4-diol. Interestingly, in spite of their apparent structural differences research has suggested similarity in action between BPA and local anesthetics such as Phenytoin (O’Reilly et al., 2012), lending credence to this distance measure’s accounting of activity-relevant similarity.

If, on the other hand, our goal was to test new chemicals that are least similar to observed chemicals, then we could choose the hold-out chemicals having the largest minimum distance to a training chemical. Assuming we chose such chemicals iteratively, we would select Iodoform (an organoiodine compound occasionally used as a disinfectant), Triethyltin bromide (an organotin compound used for proteomics research), and Indeno(1,2,3-*cd*)pyrene (an aromatic hydrocarbon that is a common environmental pollutant). That these chemicals are the most distant in  $\eta$  space from both the training set and each other suggests that the model considers them to have distinctive activity relevant variability. See Figure 16 for their structure diagrams; the predicted activity for Indeno(1,2,3-*cd*)pyrene is also shown in Figure 18.

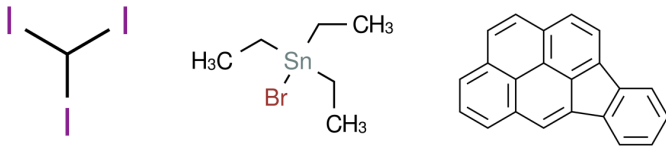


Fig 16: From left to right: Iodoform, Triethyltin bromide, and Indeno(1,2,3-*cd*)pyrene.

**4.4. Prediction.** Overall, the MSE between the data and the predicted dose-response profiles is 0.25 for the training chemicals and 0.29 for the hold-out chemicals. The 95% pointwise credible intervals cover 91.4% of the training data and 89.5% of the hold-out data, respectively. Unsurprisingly, hold-out chemicals having lower coverage also tend to have higher MSE. The pointwise coverage for specific hold-out chemicals is inversely related to the minimum distance between that chemical and its closest neighboring training chemical, while the MSE is directly related to the minimum distance between that chemical and its closest neighboring training chemical. That is, as a hold-out chemical moves farther away from other training chemicals, on average its coverage and MSE become worse.

We say a chemical is predicted to be activating, i.e. to increase activity, if the lower bound of the 95% posterior credible interval for the predicted dose response curve exceeds zero at any point. Figures 17 and 18 show model predicted mean dose-response (MDR) curves along with samples of the AC50 value, i.e. the dose at which the dose response curve is at half of its maximal value, for activating hold-out chemicals. The predicted mean and 95% posterior credible intervals for the MDR curves are smooth due to the underlying structure of  $\Lambda$ . The proportion of hold-out chemicals deemed activating by our model is nearly twice as high among the population of chemicals that are heavily tested (i.e., that have 10 or more observations). Since chemicals that are known to have toxic effects tend to be more heavily tested, this finding is suggestive of the model’s capability to detect activity.

Although the predictive ability of the model is imperfect (e.g., Bisphenol B in Figure 17 is under-predicted), overall performance appears reasonable. Particularly poorly predicted chemicals, examples of which are shown in the Supplemental Materials, tend to have shapes that differ from the common profiles and/or be farther in  $\eta$  space from training data than well-predicted curves. Also note that although the observations above the reported cytotoxicity limit were removed prior to running the model, the hormesis shape (i.e., the downturn at the end of the predicted dose response profile) remains prominent in highly activating chemicals because it is a feature of the first column of  $\Lambda$ , which has the highest column norm and drives large scale variation across profiles.

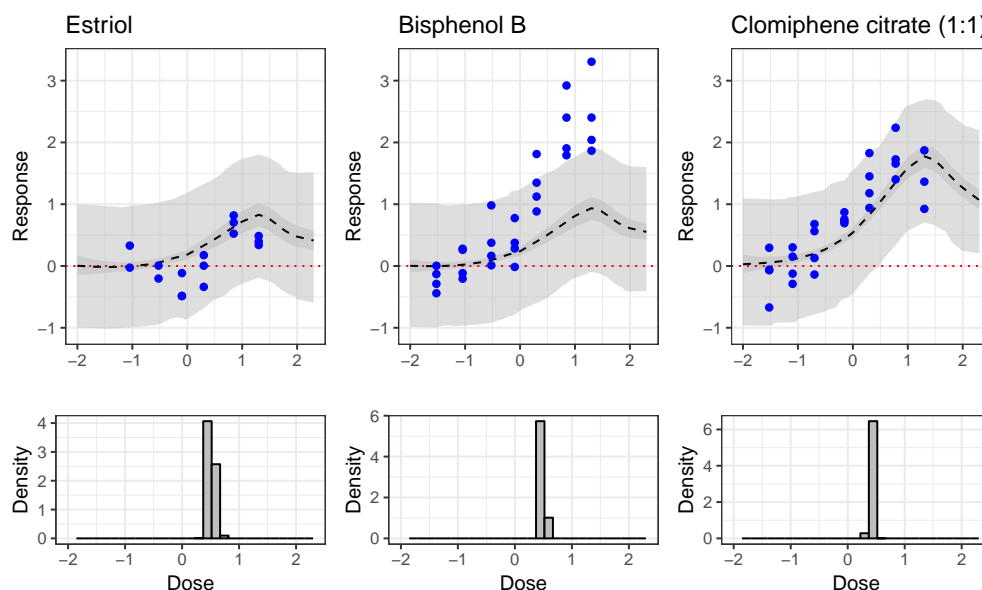


Fig 17: Results for heavily tested hold-out chemicals predicted by the model to be activating. MSEs from left to right are 0.14, 0.91, and 0.19. Top: Predicted average dose-response curve (dashed black line), 95% credible interval for expected dose-response curve (darker grey ribbon), and 95% credible interval for observed data (lighter grey ribbon). Data (held out in training) are solid blue points. Bottom: Posterior samples of the AC50 value, i.e. the dose at which the dose response curve is at half of its maximal value.

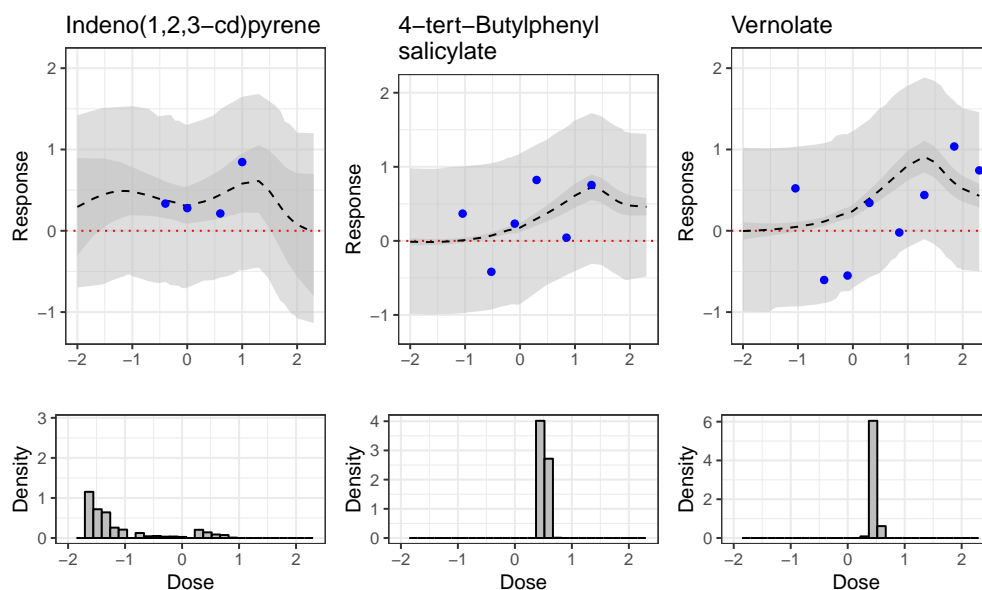


Fig 18: Results for hold-out chemicals predicted by the model to be activating. MSEs from left to right are 0.03, 0.15, and 0.30. Top: Predicted average dose-response curve (dashed black line), 95% credible interval for expected dose-response curve (darker grey ribbon), and 95% credible interval for observed data (lighter grey ribbon). Data (held out in training) are solid blue points. Bottom: Posterior samples of the AC50 value, i.e. the dose at which the dose response curve is at half of its maximal value.

In the context of this experiment, we say a chemical is predicted not to increase activity, i.e. to be non-activating, if the lower bound of the 95% posterior credible interval for the predicted MDR curve does not exceed zero at any point. Figure 19 shows model predicted non-activating dose-response curves for hold-out chemicals. As before, the predictions are smooth and appear reasonable relative to the true data. On average, hold-out chemicals deemed non-activating under the criteria outlined above have a lower maximum observed response than those deemed activating.

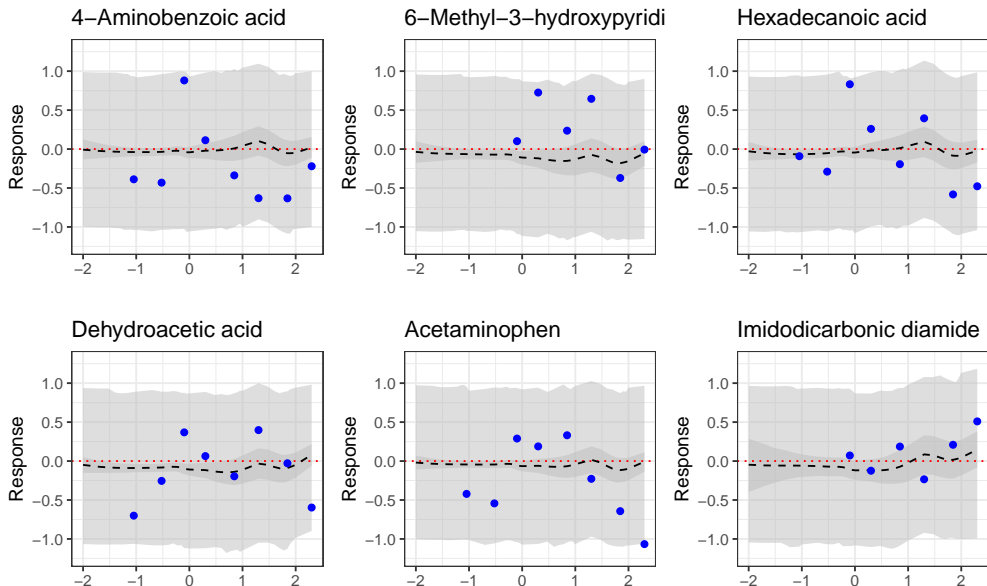


Fig 19: Results for select hold-out chemicals predicted by the model to be non-activating. MSEs from left to right, top to bottom, are 0.27, 0.24, 0.19, 0.16, 0.27, 0.06, and 0.03. Shown are predicted average dose-response curve (dashed black line), 95% credible interval for expected dose-response curve (darker grey ribbon), and 95% credible interval for observed data (lighter grey ribbon). Data (held out in training) are solid blue points.

The choice of how to prioritize chemicals for future evaluation is flexible. Assuming there are in fact no dose-response data for the hold-out chemicals, a simple scheme by which chemicals could be selected for *in vitro* study based on their BS<sup>3</sup>FA predictions would be to screen all chemicals for which the lower limit of the  $1 - \alpha$  posterior credible interval for the MDR curve exceeds some threshold (e.g., 0). The value of  $\alpha$  could be selected with attention to the resources available—a larger  $\alpha$  would lead to more chemicals being screened, whereas a smaller  $\alpha$  would mean only those chemicals the model is most confident about would be screened. Once the set of chemicals are selected for further testing, the order of screening could be determined by chemicals’ expected AC50 value, by the maximum value of their predicted MDR curves, by the highest value taken by the lower  $\alpha/2$  credible interval for expected response, by their proximity in latent space to known toxic chemicals, or by another metric of interest.

For example, if one chooses  $\alpha = 0.05$ , then 77% of hold-out chemicals have predicted dose response curve lower bound that at some point exceeds 0. The 5 highest priority chemicals using the max lower bound method would be Clomiphene citrate (1:1), Chlorethoxyfos, Surinabant, SSR 241586 HCl, and MK-578. Clomiphene citrate (1:1) (activity shown in Figure 17), the most well studied chemical on this priority list, is a selective estrogen receptor modulator used to treat ovulatory dysfunction in women trying to become pregnant. The closest neighbors to Clomiphene citrate (1:1) in the training set are Toremifene citrate (also used clinically), Fenvalerate (an insecticide),



Butachlor (an herbicide), and Chlorotrianisene (formerly used clinically). These chemicals all have known estrogenic effects (Chlorotrianisene is actually a synthetic estrogen itself) (Nulsen, Carmon and Hendrick, 1953; Go et al., 1999; Iouffe, 2000; Chang et al., 2012).

**5. Conclusion.** We have focused on the utility of distance learning for designing future chemical test sets, but these pairwise distance matrices could be used in place of Euclidean distance in any distance-based statistical analysis. This would include distance-based clustering of chemicals, as well as kernel and Gaussian process-based models. As a specific example, the authors believe these activity-relevant distances have the potential to improve main effects estimates in mixture models for human health outcomes. It is likely that incorporating knowledge about similarity in activity-relevant space (e.g., by using the toxicity-relevant pairwise distance matrix to inform a group penalized regression model) would provide stabilization for main effects, and in turn allow for better estimation of the interaction effects.

The designation of activating vs. not-activating in the BS<sup>3</sup>FA model is based on a posterior summary of the predicted dose-response profiles; there is no direct incorporation of the concept of a chemical being inactive in the model itself. It may be desirable, particularly when considering assays having very few chemicals presenting with any activity, to probabilistically model inactivity. For example, the dose response profile could be modeled as a mixture between the zero-vector and the BS<sup>3</sup>FA factor model, with a learned weight on the zero vector corresponding to the probability of inactivity.

The BS<sup>3</sup>FA model deals with the structured decomposition of a single assay and a single feature data set. In reality, any sort of model hoping to extend to human health outcomes will need to utilize information from multiple sources. In the ToxCast data set, there is not just one dose-response curve per chemical. There are many assay endpoints of potential relevance to human toxicity. Furthermore, there are potentially many useful chemical feature descriptors (we used Mold2, but others include MACCS keys, Daylight Fingerprints, or Morgan Fingerprints, to name a few). Future work will link the ideas in BS<sup>3</sup>FA to those in (Wilson, Reif and Reich, 2014) to allow for a more direct activating/non-activating assignment and to hierarchically describe variability across multiple assays. Extending even further, the holy grail of toxicity modeling would be an explicit linking of multiple assay endpoints to human health data, such that human health outcomes could be predicted from chemical structure alone.

**6. Acknowledgements.** This work was partially supported by the National Institute of Environmental Health Sciences of the United States National Institutes of Health (grants 1R01ES028804-01 and 5R01ES027498-02) and the Department of Energy Computational Science Graduate Fellowship (grant DE-FG02-97ER25308). The funders had no role in study design, data collection and analysis, decision to publish, or preparation of the manuscript. The authors would like to thank Evan Poworoznek and Bora Jin for helpful comments. Matthew W. Wheeler is a co-author pending approval from the National Institute for Occupational Safety and Health.

## References.

- BARBER, R. F., REIMHERR, M., SCHILL, T. et al. (2017). The function-on-scalar LASSO with applications to longitudinal GWAS. *Electronic Journal of Statistics* **11** 1351–1389.
- BHATTACHARYA, A. and DUNSON, D. B. (2011). Sparse Bayesian infinite factor models. *Biometrika* 291–306.
- CANALE, A. and DUNSON, D. B. (2013). Nonparametric Bayes modelling of count processes. *Biometrika* **100** 801–816.

- CARVALHO, C. M., POLSON, N. G. and SCOTT, J. G. (2010). The horseshoe estimator for sparse signals. *Biometrika* **97** 465–480.
- CHANG, J., GUI, W., WANG, M. and ZHU, G. (2012). Effects of butachlor on estrogen receptor, vitellogenin and P450 aromatase gene expression in the early life stage of zebrafish. *Journal of Environmental Science and Health, Part A* **47** 1672–1677.
- CHEN, Y., GOLDSMITH, J. and OGDEN, R. T. (2016). Variable selection in function-on-scalar regression. *Stat* **5** 88–101.
- DIX, D. J., HOUCK, K. A., MARTIN, M. T., RICHARD, A. M., SETZER, R. W. and KAVLOCK, R. J. (2006). The ToxCast program for prioritizing toxicity testing of environmental chemicals. *Toxicological Sciences* **95** 5–12.
- DURANTE, D. (2017). A note on the multiplicative gamma process. *Statistics & Probability Letters* **122** 198–204.
- FAN, Z. and REIMHERR, M. (2017). High-dimensional adaptive function-on-scalar regression. *Econometrics and Statistics* **1** 167–183.
- GO, V., GAREY, J., WOLFF, M. S. and POGO, B. (1999). Estrogenic potential of certain pyrethroid compounds in the MCF-7 human breast carcinoma cell line. *Environmental Health Perspectives* **107** 173–177.
- HONG, H., XIE, Q., GE, W., QIAN, F., FANG, H., SHI, L., SU, Z., PERKINS, R. and TONG, W. (2008). Mold2, molecular descriptors from 2D structures for chemoinformatics and toxicoinformatics. *Journal of Chemical Information and Modeling* **48** 1337–1344.
- HONG, H., SLAVOV, S., GE, W., QIAN, F., SU, Z., FANG, H., CHENG, Y., PERKINS, R., SHI, L. and TONG, W. (2012). Mold2 molecular descriptors for QSAR. *Statistical Modelling of Molecular Descriptors in QSAR/QSPR* **2** 65–109.
- JUDSON, R. S., HOUCK, K. A., KAVLOCK, R. J., KNUDSEN, T. B., MARTIN, M. T., MORTENSEN, H. M., REIF, D. M., ROTROFF, D. M., SHAH, I., RICHARD, A. M. et al. (2009). In vitro screening of environmental chemicals for targeted testing prioritization: the ToxCast project. *Environmental Health Perspectives* **118** 485–492.
- KAVLOCK, R., CHANDLER, K., HOUCK, K., HUNTER, S., JUDSON, R., KLEINSTREUER, N., KNUDSEN, T., MARTIN, M., PADILLA, S., REIF, D. et al. (2012). Update on EPA’s ToxCast program: providing high throughput decision support tools for chemical risk management. *Chemical Research in Toxicology* **25** 1287–1302.
- KLIEWER, S. A., GOODWIN, B. and WILLSON, T. M. (2002). The nuclear pregnane X receptor: a key regulator of xenobiotic metabolism. *Endocrine Reviews* **23** 687–702.
- KNOWLES, D., GHAHRAMANI, Z. et al. (2011). Nonparametric Bayesian sparse factor models with application to gene expression modeling. *The Annals of Applied Statistics* **5** 1534–1552.
- KOWAL, D. R. and BOURGEOIS, D. C. (2018). Bayesian function-on-scalars regression for high dimensional data. *arXiv preprint arXiv:1808.06689*.
- LI, G., SHEN, H. and HUANG, J. Z. (2016). Supervised sparse and functional principal component analysis. *Journal of Computational and Graphical Statistics* **25** 859–878.
- LIU, R., RALLO, R., GEORGE, S., JI, Z., NAIR, S., NEL, A. E. and COHEN, Y. (2011). Classification NanoSAR development for cytotoxicity of metal oxide nanoparticles. *Small* **7** 1118–1126.
- LOCK, E. F., HOADLEY, K. A., MARRON, J. S. and NOBEL, A. B. (2013). Joint and individual variation explained (JIVE) for integrated analysis of multiple data types. *The Annals of Applied Statistics* **7** 523.
- LOUFFE, L. (2000). Selective estrogen receptor modulators (SERMs) in clinical practice. *Journal of the Society for Gynecologic Investigation* **7** S38–S46.
- LOW-KAM, C., TELESKA, D., JI, Z., ZHANG, H., XIA, T., ZINK, J. I., NEL, A. E. et al. (2015). A Bayesian regression tree approach to identify the effect of nanoparticles’ properties on toxicity profiles. *The Annals of Applied Statistics* **9** 383–401.
- MAKALIC, E. and SCHMIDT, D. F. (2016). A simple sampler for the horseshoe estimator. *IEEE Signal Processing Letters* **23** 179–182.
- MARTIN, Y. C., KOFRON, J. L. and TRAPHAGEN, L. M. (2002). Do structurally similar molecules have similar biological activity? *Journal of Medicinal Chemistry* **45** 4350–4358.
- MENG, J., ZHANG, J., QI, Y., CHEN, Y. and HUANG, Y. (2010). Uncovering transcriptional regulatory networks by sparse Bayesian factor model. *EURASIP Journal on Advances in Signal Processing* **2010** 3.
- NIKOLOVA, N. and JAWORSKA, J. (2003). Approaches to measure chemical similarity—a review. *QSAR & Combinatorial Science* **22** 1006–1026.
- NULSEN, R. O., CARMON, W. B. and HENDRICK, H. O. (1953). Tace (chlorotrianisene), a new estrogen for inhibition of lactation. *American Journal of Obstetrics & Gynecology* **65** 1048–1051.
- O’REILLY, A. O., EBERHARDT, E., WEIDNER, C., ALZHEIMER, C., WALLACE, B. and LAMPERT, A. (2012). Bisphenol A binds to the local anesthetic receptor site to block the human cardiac sodium channel. *PLoS One* **7** e41667.
- PATEL, T., TELESKA, D., LOW-KAM, C., JI, Z., ZHANG, H. Y., XIA, T., ZINC, J. I. and NEL, A. (2014). Relating nano-particle properties to biological outcomes in exposure escalation experiments. *Environmetrics* **25** 57–68.
- PATI, D., BHATTACHARYA, A., PILLAI, N. S., DUNSON, D. et al. (2014). Posterior contraction in sparse Bayesian factor models for massive covariance matrices. *The Annals of Statistics* **42** 1102–1130.

- WEININGER, D. (1988). SMILES, a chemical language and information system. 1. Introduction to methodology and encoding rules. *Journal of Chemical Information and Computer Sciences* **28** 31–36.
- WHEELER, M. W. (2019). Bayesian additive adaptive basis tensor product models for modeling high dimensional surfaces: an application to high-throughput toxicity testing. *Biometrics* **75** 193–201.
- WILSON, A., REIF, D. M. and REICH, B. J. (2014). Hierarchical dose–response modeling for high-throughput toxicity screening of environmental chemicals. *Biometrics* **70** 237–246.
- YOSHIDA, R. and WEST, M. (2010). Bayesian learning in sparse graphical factor models via variational mean-field annealing. *Journal of Machine Learning Research* **11** 1771–1798.